HHS Public Access

Author manuscript

Bioconjug Chem. Author manuscript; available in PMC 2020 June 12.

Published in final edited form as:

Bioconjug Chem. 2019 February 20; 30(2): 476–486. doi:10.1021/acs.bioconjchem.8b00696.

Pathways governing polyethylenimine (PEI) polyplex transfection in microporous annealed particle (MAP) scaffolds

Norman Truong[1], **Sasha Cai Lesher-Pérez**[1], **Evan Kurt**[2], **Tatiana Segura**[1,3]

[1]Department of Chemical and Biomolecular Engineering, University of California Los Angeles, Los Angeles, CA 90095

[2]Department of Biomedical Engineering, Duke University, Durham, NC 27708

[3]Current affiliations: Departments of Biomedical Engineering, Neurology, and Dermatology, Duke University, Durham, NC 27708

Abstract

Gene delivery using injectable hydrogels can serve as a potential method for regulated tissue regeneration in wound healing. Our microporous annealed particle (MAP) hydrogel has been shown to promote cellular infiltration in both skin and brain wounds, while reducing inflammation. Although the scaffold itself can promote healing, likely other signals will be required to promote healing of hard to treat wounds. Gene delivery is one approach to introduce desired bioactive signals. In this study, we investigated how the properties of MAP hydrogels influence non-viral gene delivery of polyethylenimine (PEI) condensed plasmid to cells seeded within the MAP gel. From past studies, we found that gene transfer to cells seeded in tissue culture plastic differed from gene transfer to cells seeded inside hydrogel scaffolds. Since MAP scaffolds are generated from hydrogel microparticles that are approximately 100μm in diameter, they display local characteristics that can be viewed as two dimensional or three dimensional to cells. Thus, we sought to study if gene transfer inside MAP scaffolds differed to gene transfer to cells seeded in tissue culture plastic. We sought to understand the roles of endocytosis pathway, actin and microtubule dynamics, RhoGTPases, and YAP/TAZ on transfection of human fibroblasts.

Graphical Abstract

Supporting Information Description

The supplemental results give more details on the transfection efficiency and GLuc expression results for the pathways explored (Figures S1–S2). The supplemental methods further describe the custom cell culturing device that was created to prepare the MAP gel and cells for transfection studies, with a schematic and model shown in Figure S3.

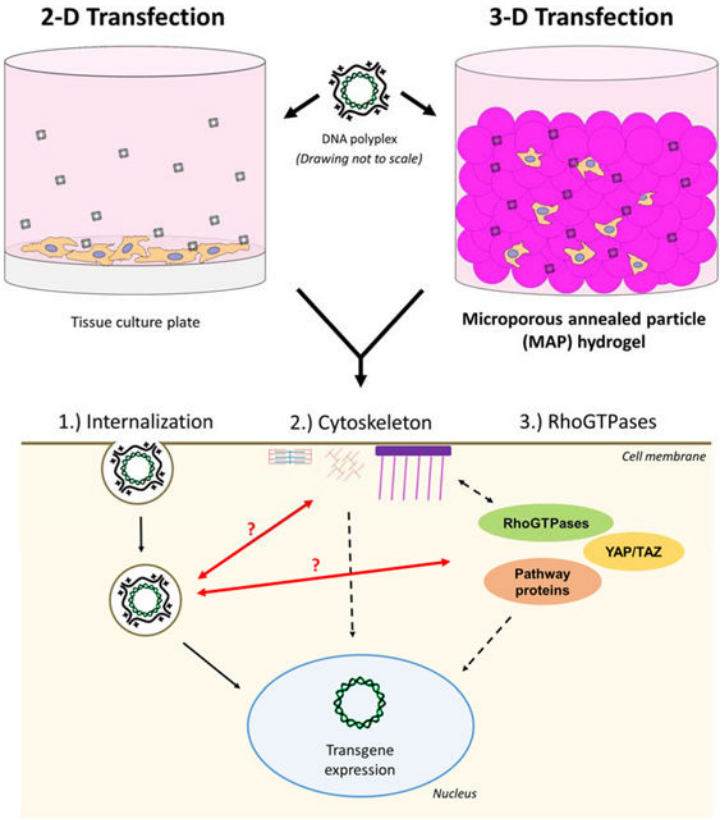

Keywords

gene delivery; non-viral; MAP hydrogel; porous; polyplex

Introduction

While non-viral gene delivery has been used in the development of therapies for tissue regeneration, its level of widespread adoption has been limited by overall low transfection efficiency. Therefore, strategies to increase the efficiency of non-viral gene delivery are critical to improving biological studies both *in vitro* and *in vivo*. While there has been considerable research done on improving gene carriers[1,2] and vector DNA constructs[3], many studies have also explored the role the cellular microenvironment on key cellular processes which influence gene transfer. Such features of the microenvironment include substrate chemistry and charge[4], extracellular matrix protein composition[5,6], cell adhesion ligand presentation and concentration[7,8], substrate stiffness[8,9], and surface topography[10]. Importantly, these key features triggered different responses when cells were seeded in two dimensions compared to in three dimensions. Culturing cells in three dimensions (3-D) in hydrogel scaffolds is crucial for biomedical applications, as it more accurately mimics the native tissue environment, serving as a better *in vitro* model to study biological processes or to test new therapies[11]. The locally observed cellular microenvironment is especially relevant to the development of new hydrogel biomaterials used to locally deliver therapeutic

genes to scaffold-infiltrating cells for regenerative medicine applications such as in wound healing, stroke recovery, cartilage and bone regeneration.

Our laboratory recently developed microporous annealed particle (MAP) hydrogels, the first injectable porous scaffold. This scaffold is composed of hydrogel microparticles (μgels) that are annealed to each other forming a granular solid. Along the boundaries of the μgels void spaces or “pores” are generated that are large enough for cell infiltration of endogenous cells *in vivo* or cell spreading and proliferation *in vitro*[12,13]. When used for cell culture in vitro, the μgels can be mixed with the cells prior to annealing such that the cells are homogenously dispersed in the gel. Using this approach we have found that MAP scaffold allows cell proliferation and extensive cell spreading throughout the scaffold differently from culture in nonporous hydrogels, as rates of cell spreading and infiltration are no longer dependent on the local cell-mediated degradation of the hydrogel[13,14]. In addition, the MAP scaffold shows significant promise in promoting tissue regeneration largely due to its inherent porous structure and the ability to seamlessly fill the wound cavity from its injectable-nature. In a murine cutaneous wound healing model, MAP scaffold injections accelerated tissue formation and vascularization[12]. Similarly, in a murine stroke model, the MAP scaffold reduced inflammation, increased peri-infarct vascularization, and induced migration of neuroprogenitor cells into the stroke site[14]. Coupling such a material with the therapeutic potential of non-viral gene delivery may yield positive outcomes for therapy development.

Since our laboratory has previously demonstrated that dimensionality affects the mechanisms by which cationic polymer-mediated gene transfer occurs[15], specifically for the commonly used linear PEI, here we sought to understand if and how gene transfer in MAP cell culture would differ from that in 2-D cell culture on tissue culture plastic. Based on previous studies in nanoporous hydrogels[15,16], the roles of endocytic pathways, cytoskeletal dynamics, and RhoGTPase-mediated signaling in transfection from cells cultured in MAP were investigated in comparison to 2-D culture (Figure 1). Ultimately, enhancing knowledge of these mechanisms will enable the development of strategies to increase gene transfer efficiency from therapeutically relevant MAP hydrogels.

Results and Discussion

Analysis of gel physical properties and cell culture in MAP scaffolds

To synthesize microgels, HA-Norb was first prepared using amine-carboxylic acid chemistry utilizing the carboxylic acid in the backbone of HA (one per monomer) and a free amine-containing norbornene molecule. NMR analysis of the modified polymer revealed that 41.9% of the HA monomers were reacted to contain the norbornene functional group. HA microgels were produced using a water-in-hexane emulsion and UV light to trigger a thiolene reaction between the norbornene groups on the HA backbone and the thiols of the DTT crosslinker. The resulting microgels were polydisperse with diameters ranging from 10 to greater than 200 μm, but are all spherical in shape (Figure 2A). To narrow down the size range, microgels were purified to remove hexane and surfactant and swelled in PBS before sieving through pore size ranges of 60–100 μm to generate a microgel population of reduced polydispersity (Figure 2B). The average diameter and standard deviation of this population was 86.0 ± 20.3 μm.

MAP scaffolds were generated by annealing microgels within a culture well using a click reaction of the norbornene groups at the surfaces of the beads and a separate 4-arm PEG-tetrazine (PEG-Tet) crosslinker. Concentrated fluorescently tagged microgels were mixed with PEG-Tet crosslinker and allowed to anneal to generate MAP scaffolds within custom PDMS culture devices (Figure 2C). The average void fraction of the porous scaffolds was determined to be 0.22 ± 0.06.

We next characterized the rheological properties of the MAP scaffolds used in this study to verify consistency with recent work and ensure that the gels were an appropriate stiffness for the cell culture. After using the crosslinking ratio of 14 mmol SH:mmol HA to generate microgels, oscillation rheometry was performed on both the nonporous gel formulation as well as the annealed MAP scaffold. The storage modulus (G') measurement of the nonporous gel formulation, measured to be 1813 ± 315 Pa (data not shown), is representative of the local microgel stiffness experienced by a cell which is adhered to a microgel, while the storage modulus of the annealed MAP scaffold, measured to be 223 ± 67 Pa, provides an overall characterization of the bulk rheological properties of the scaffold as a whole (Figure 2D). We believe that taken together, these two measurements provide a more comprehensive characterization which is relevant to cell mechanosensing of the microenvironment.

Lastly, the spreading of human dermal fibroblasts and subsequent transfection in the MAP scaffolds were visually assessed through seeding cells in the MAP scaffold, annealing the microgels, culturing, and fixing and staining (Figure 3A and 3B). At day 2 of culture, substantial spreading was observed, showing that the cells were sufficiently acclimated to the 3-D scaffold. Following cell growth in the 3-D culture, cells were transfected with jetPEI polyplexes to characterize polyplex diffusion into the gel and uptake by cells (Figure 3C). Plasmid DNA was mixed with the fluorescent intercalating dye, YOYO-1. There is concern for polyplex interactions within hyaluronic acid (HA) gels since the charged interactions have been shown *in vitro* to induce polyplex aggregation[22,23], aside from the PEG-Tet crosslinker and steric interactions[15,24]. Based on confocal microscopy and z-stacks, the percent co-localization of YOYO-1 polyplexes was visually observed in IMARIS (Figure 3D and 3E), and then quantified for the distribution relative to seeded cells based on overlapping regions of fluorescence (Figure 3F). As shown, diffusional limitations were negligible as the polyplexes were able to be fully distributed throughout the gel and localize closely with that of the cells, with a total co-localization of 35.1% and an average of 18.0 ± 5.1% across the entire gel volume.

Analyzing dependence of endocytic, cytoskeletal, RhoGTPase, and YAP/TAZ pathways on transfection

We wanted to study the role of various pathways and processes, specifically those contributing to endocytosis, cytoskeletal dynamics, and RhoGTPase- and YAP/TAZ-mediated pathways, in gene transfer in MAP gel culture compared to cells plated in 2-D on conventional 2-D tissue culture plastic (Figure 3C). Previous studies have demonstrated in both 2-D and 3-D culture that transfection occurs preferentially through specific endocytic pathways and that the nature of the dependence differs as a function of dimensionality[6,15].

Micropinocytosis, caveolae-mediated endocytosis, and clathrin-mediated endocytosis were directly and indirectly inhibited using various chemical inhibitors which were administered before and during transfection (Figure 1). It was determined that inhibition of micropinocytosis and caveolae-mediated endocytosis enhanced transgene expression in 2-D but decreased transgene expression in MAP gels (Figure 4). Direct inhibition of clathrin-mediated endocytosis using chlorpromazine significantly decreased transgene expression in both 2-D and MAP culture conditions, while there was no significant effect with indirect inhibition of dynamin via dynasore treatment. However, from this and past studies, transfection within hydrogels is less efficient than direct 2-D transfections[22,25], with approximately 10-fold less expression from MAP based on the Relative Luminescence Units for the luciferase assay (Figure S1). Due to the differences and wanting to infer clear trends on the mechanism rather than simply transfection efficiency, as this had been covered in our previous work, the data was normalized with respect to the “no treatment” control for each 2-D or MAP conditions (Figure 4). Together these findings suggest that gene transfer in 2-D predominantly occurs through clathrin-mediated endocytosis, while the more consistent suppression of gene transfer in MAP culture across all endocytic pathways suggests that gene transfer in MAP is dependent not only on clathrin-mediated endocytosis, but also to some extent on micropinocytosis and caveolae-mediated endocytosis. A previous study investigating the effects of inhibition of endocytic pathways in D1 mouse mesenchymal stem cells observed a dependence of gene transfer on both caveolae- and clathrin-mediated endocytosis in both 2-D and nonporous 3-D hydrogels[15]; however, the dominant internalization route of polyplexes seems to be cell line dependent, suggesting that comparisons drawn between findings in different cell lines may not necessarily be true[26].

The role of cytoskeletal dynamics in gene transfer in MAP gels and 2-D culture was studied by inhibiting actin, myosin, and microtubule dynamics (Figure 1). Previous studies have illustrated the importance of cytoskeletal activity in gene transfer mechanisms, mostly in 2-D culture[16,27,28]. While there was no significant effect of inhibition of actin polymerization via cytochalasin D, expression significantly decreased with jasplakinolide administration (Figure 5). Jasplakinolide enhances the frequency of actin nucleation; however, it does so at the expense of actin polymeric organization, adversely affecting endosomal trafficking[29]. This suggests that organized actin polymerization may be necessary for transfection in MAP gels, but not so for 2-D culture. Stabilization of microtubules with paclitaxel enhanced transgene expression both in 2-D and in MAP gels, while inhibition of microtubule polymerization with nocodazole resulted in a decrease in expression, suggesting a strong dependence of polyplex trafficking on microtubule dynamics. Previous reports have also similarly identified the importance of microtubules in the trafficking of polyplexes towards the nucleus[27,28,30].

Next, the roles of the RhoGTPases Rho, Rac, and Cdc42 in the gene transfer process were investigated (Figure 1). Rho proteins are GTPases which regulate a variety of cell processes but play an integral role in mediating integrin binding to the cell’s ECM and actin cytoskeletal and microtubule dynamics in response to that[16,31]. The Rho, Rac, and Cdc42 GTPases have previously been shown to regulate cell polarity, lamellipodial protrusion, and cell adhesion during migration in 2-D[18]. Inhibition, activation, and overexpression of RhoGTPases have also been shown to modulate the intracellular processing of polyplexes in

2-D[16]. Here, inhibition of RhoA/B/C using C3 transferase significantly decreased transgene expression in MAP gels, with a nonsignificant effect in 2-D (Figure 6). A similar pattern was seen in the inhibition of ROCK, a downstream effector of RhoA. However, inhibition of PAK1, a downstream effector of Rac and Cdc42, with IPA-3 increased transgene expression in 2-D but decreased expression in MAP gels, suggesting a difference in gene transfer mechanism between 2-D and MAP gels. Activation of Rho, Rac, and Cdc42 resulted in a significant increase in transfection in MAP gels but no significant effect in 2-D. However, the activation of RhoA/B/C resulted in a decrease in transgene expression in both 2-D and MAP gels, suggesting that the activation of Rac and Cdc42 may be more integral to gene transfer in MAP gels.

It was noted that both Rac and Cdc42 have separate activities on actin polymerization; however, there are currently no suitable methods to differentiate between Rac and Cdc42 activation due to their similarity in function for agonists and relation to the Rho pathway[16,17,32–34]. We were able to identify a candidate agonist that was specific for Rho (A/B/C), which did not have effects on Rac/Cdc42 activity[15,16]. Some studies have been able to isolate the actin behavior by knocking-out Rho or Rac[32], but this causes many other phenotypic changes that would prevent accurate results in our MAP hydrogels. A few agonists have been identified for Rac and RhoA[17,34], excluding Cdc42 effects, but this still does not distinguish between the remaining two. Should agonists be developed for Rac and Cdc42 that can distinguish their separate activities from RhoA, it would be a valuable contribution the understanding the endocytosis mechanism. In addition, the effect of Rho/Rac/Cdc42 is dependent on the cell infiltration and spreading within the hydrogel, which varies based on its physical properties. As we have previously shown, the transfection efficiency changes based on the local environment, aside from using other hydrogel scaffold systems such as pre-cast porous[15,25] or nanoporous[16,22] hydrogels. Due to the many variables involved in generating MAP gels, from bead stiffness, porosity, RGD clustering, size, and resulting void space, only one set of parameters was selected for this study to be characterized for the pathway differences that regulate transgene uptake and expression. This follows previous work that shows similar effects from the Rho/Rac/Cdc42 inhibitors and activators[16], but the trends do vary since the scaffold changes how cells interact. Future studies may look to other gel parameter conditions and see how that affects the pathway response differently, given that the end transfection efficiency does differ.

Lastly, the role of YAP/TAZ (Yes-associated protein/Transcriptional coactivator with PDZ-binding motif), a key sensor and regulator of cell mechanotransduction[21,35], in gene transfer was studied (Figure 1). YAP/TAZ relays extracellular mechanical cues to the nucleus, thereby triggering downstream pathways[36]. It has been shown to play an integral role in the stiffness-dependent differentiation of mesenchymal stem cells and in fibroblast activation and fibrogenesis as a function of substrate stiffness[21,37], and YAP/TAZ nuclear localization has been shown to be correlated with the extent of cell spreading[36]. Given that multiple studies have reported a consistent correlation between cell spreading and gene transfer, we next investigated whether gene transfer is dependent on YAP/TAZ-mediated signaling, which has not been studied prior to this study. YAP was inhibited with the administration of verteporfin, which upregulates a chaperon protein that localizes YAP in the cytoplasm and targets it for degradation[38]. Inhibiting YAP resulted in a dramatic decrease in transgene

expression in both 2-D and MAP gels to near-zero levels (Figure 6), demonstrating that YAP/TAZ signaling is integral to gene transfer. The dependence of gene transfer on stiffness and cell adhesion ligand presentation may also be mediated by YAP/TAZ, but further studies will need to be conducted to verify this mechanism. The YAP/TAZ relation to the Rho/Rac/Cdc42 endocytosis mechanism has only been understood so far through actin dynamics; however, several targets would be beneficial to evaluate and determine their role in the endocytosis pathway between 2-D and MAP, including the Rho activator AKAP-Lbc[20] and Rho-ROCK effector CFL[39], apart from indirect actin regulation via TEAD[38,40,41]. Future studies may help to evaluate which mechanism is used specifically in endocytosis to relate RhoA directly to YAP regulation and resulting microtubule effects for cell spreading.

Conclusions

In this study, we performed *in vitro* studies to examine pathways responsible for polyplex-mediated gene transfer in a 3-D MAP scaffold as compared to standard 2-D culture. By analyzing the role of endocytic pathways, cytoskeletal dynamics, and RhoGTPases and YAP/TAZ, which are important downstream mediators of integrin signaling, we determined that: (1) clathrin-mediated endocytosis is less dominant in driving gene transfer in MAP gels than in 2-D culture; (2) as in 2-D culture, microtubule dynamics are integral to polyplex trafficking and efficiency of gene transfer; (3) Rac and Cdc42 may be important to the efficiency of polyplex-mediated gene transfer; and (4) as in 2-D culture, YAP activity is crucial to enabling gene transfer. These findings will help to improve non-viral gene delivery methods from our therapeutically relevant MAP scaffolds by influencing cell pathway response, enhancing transfection and tissue repair *in vivo*.

Methods

Preparation of hyaluronic acid-norbornene (HA-Norb)

As depicted in Figure 7A, to modify hyaluronic acid (HA) to contain norbornene functional groups, 1 g of 60 kDa sodium hyaluronan (Genzyme, Cambridge, MA) and 3.111 g 4-(4,6-dimethoxy-1,3,5-triazin-2-yl)-4-methyl-morpholinium chloride (DMTMM) (Thermo Fisher Scientific, Waltham, MA) were each dissolved in 40 mL 200 mM MES buffer pH 5.5. The two solutions were combined and stirred for 10 min to allow for activation of the carboxylic acid. 0.677 mL 5-norbornene-2-methylamine (TCI America, Portland, OR) was added dropwise to the reaction mixture, which was then allowed to react overnight at 25°C with constant stirring. The reaction product was then precipitated in ethanol, filtered to collect the solid, dissolved in 2 M NaCl in water, and dialyzed under running deionized water for 24 hours. The final product was then filtered, flash-frozen, and lyophilized. The extent of modification was confirmed via ^{1}H-NMR spectrometry. ^{1}H NMR shifts of attached norbornene groups in the product in D2O are δ = 6.33 and 6.02 (vinyl protons, endo), and 6.26 and 6.23 ppm (vinyl protons, exo). The integrations of these peaks were normalized to the peak corresponding to the methyl group on the HA monomer at δ = 2.0 ppm to determine percent of HA monomers modified to contain norbornene groups.

Synthesis of polyethylene glycol-tetrazine (PEG-tet)

PEG-tet was synthesized by combining 100 mg 4-arm 20kDa PEG-thiol (NOF America, White Plains, NY) and 15 mg methyltetrazine-PEG_4-maleimide (Kerafast, Boston, MA), each dissolved in 0.5 mL dichloromethane (DCM). 1 μL of trimethylamine was added and the mixture was allowed to stir at 25°C for 4 hours while protected from light. The reaction product was precipitated in 50 mL of cold diethyl ether and allowed to dry under vacuum overnight.

HA microgel formation and purification

As depicted in Figure 7B, HA-Norb microgels were prepared using a batch water-in-hexane emulsion technique. 1 mL of gel precursor solution was prepared in HEPES buffer pH 8.3 with HA-Norb at a final concentration of 3.5 wt%, lithium phenyl(2,4,6-trimethylbenzoyl)phosphinate photo-initiator (LAP; TCI America) at 2.2 mM, thiolated RGD peptide (RGDSPGERCG; Genscript, Piscataway, NJ) at 500 μM, and tris(2-carboxyethyl)phosphine (TCEP) at 25% of the total thiol molarity (i.e. mmol TCEP:mmol thiols = 1:4). Once all the components were mixed, a 50 mM stock of dithiothreitol (DTT) (Thermo Fisher Scientific) was added as the crosslinker to achieve a crosslinking ratio (mmol SH/mmol HA) of 14. For RGD clustering, a portion of the HA-Norb was combined with the total amount of RGD peptide and pre-reacted by exposing the solution to UV light for 1 minute at 10 mW/cm^2 in the presence of the appropriate amount of LAP and TCEP, after which the remaining HA-Norb, LAP, and TCEP were added, along with DTT. This final gel precursor solution was then pipetted into a round-bottom flask containing 10 mL 3% span-80 in hexane continuously stirring at 800 rpm, then mixed by pipetting up and down 9 times to generate a stable emulsion. The flask's contents were then purged with argon and exposed to UV light at 15 mW/cm^2 for 10 minutes to trigger the norbornene-thiol crosslinking reaction to form microgels.

Next, the crosslinked microgels in hexane was transferred into a conical tube and centrifuged at 1000 × g and washed with hexane three times. The microgels were then transferred to 1% Pluronic F107 in PBS for 30 min to allow for swelling before sieving using 200μm, 100μm, 60μm, and 20μm (PluriSelect, Leipzig, Germany) pore size strainers. During sieving, microgels were washed with 10mL 1% Pluronic in PBS and 50mL PBS. The collected microgels were then autoclaved and pelleted by centrifugation at 14000 × g for 5 minutes, after which the supernatant was removed and microgels were stored at 4°C until further use.

Microgel size distribution

After sieving and tagging with fluorophore, free microgels in PBS were imaged as z-stacks using confocal microscopy using a 10x objective to obtain a maximum intensity projection. These images were then analyzed using the particle analysis toolkit in ImageJ to obtain diameter measurements of 1300 microgels.

Microgel annealing to generate MAP scaffolds

A 5.32 mM solution of PEG-Tet in PBS was mixed with microgels at a 1:6 volumetric ratio of PEG-Tet to microgels and immediately centrifuged at 14000 × g for 3 min. Excess liquid

was removed, and 15 μL of gel was pipetted into each well and allowed to anneal for 1 hour at 37°C.

Preparation of cell culturing devices

A custom negative mold was printed using a 3-D, Form 2 stereolithography printer (Formlabs, Inc.). Cell culture devices were cast using soft lithography to produce a PDMS reservoir for cell culture. The culture wells were composed of a cylindrical culture section (3 mm in diameter and 5 mm tall), enabling a maximum of 35 μL of volume. Additionally, a conical media reservoir above the cylindrical culturing section was able to contain up to 150 μL of media. Specific dimensions of the mold, and subsequently the PDMS wells, can be found in Figure S3. To fabricate PDMS culturing devices, 70 g of Sylgard 184 PDMS (Dow Corning) was preparing according to the manufacturer's instructions and poured into a 10 cm × 10 cm square dish. The mold was placed in the PDMS, and the PDMS was degassed by applying a vacuum for 1 hour. Subsequently, the PDMS was allowed to cure at 60°C for 4 hours in a convection oven. The PDMS slab was then cut into three-well pieces and plasma-bonded to cover glass slides using a corona plasma gun. PDMS triplicate well-slides were then autoclaved prior to use for cell culture and experimental evaluation.

Void space analysis

Annealed MAP scaffolds of various microgel bead sizes were incubated with PBS containing 1 μg/mL 500 kDa tetramethylrhodamine isothiocyanate-dextran (TRITC-dextran) (Sigma-Aldrich, St. Louis, MO) to fill the void space in between microgels, as it is too large to penetrate the microgel's polymer network. The labelled void space was imaged using confocal microscopy to obtain 200-μm z-stacks. The z-stacks were imported into IMARIS to generate surface renders, and void space volumes were quantified as a fraction of the total volume represented by the z-stack. A minimum of four measurements were made for each MAP scaffold.

Oscillation rheometry

Stiffness of both nonporous HA-Norb hydrogels and of annealed MAP gels were measured as the storage modulus (G') using a plate-to-plate rheometer (Physica MCR, Anton Paar, Ashland, VA). To create a nonporous HA-Norb gel, 45 μL of the gel precursor solution was prepared as described previously and pipetted onto a Sigmacote-treated (Sigma-Aldrich) glass slide. 1mm-thick spacers were placed on either side of the slide and a second Sigmacote-treated slide was placed on top to sandwich the gel precursor solution and fastened into place using binder clips. The gel was exposed to UV light at 15 mW/cm^2 for 1 minute, then flipped and exposed for another minute for uniform crosslinking. The crosslinked gel was transferred into PBS and allowed to swell overnight. A frequency sweep was performed on the hydrogels using a strain of 0.2% with an angular frequency range of 0.5 to 10 rad/s. To measure the storage modulus of an annealed MAP gel, 50 μL microgels with PEG-Tet were pipetted directly onto the rheometer stage. The measuring position was set to 1mm and the gel was allowed to incubate with humidity for 1 hour to allow for annealing. Once the gel was annealed, a frequency sweep was performed on the hydrogels using a strain of 1% with an angular frequency range of 0.5 to 10 rad/s.

Cell culture and seeding HDFs in MAP scaffolds

Human dermal fibroblasts (HDF; Cell Applications, Inc., San Diego, CA) were maintained in culture in Dulbecco's modified Eagle's medium (Thermo Fisher Scientific) containing 10% fetal bovine serum (Thermo Fisher Scientific) at 37°C and 5% CO_2. Media was changed every 2–3 days.

To seed cells in MAP scaffolds, 100 μL microgels were first equilibrated in supplemented media for 30 minutes before pelleting and removing supernatant. HDFs were trypsinized and 1.2×10^5 cells were pelleted by centrifugation at 250 × g for 5 minutes. Media supernatant was aspirated, and equilibrated microgels in PEG-Tet solution (prepared as previously described) were then added to the cell pellet and mixed thoroughly by pipetting. Importantly, prior to gel/cell seeding, 6 μL of sterile 1% agarose in PBS was added to the wells to coat the glass surface and allowed to cool to 25°C to prevent cell attachment to glass. 15 μL of gel plus cells was then pipetted into each well in the PDMS culturing device. The MAP gel was allowed to anneal for 1 hour at 37°C. After annealing, the wells were filled with 150 μL supplemented media containing 50 μg/mL primocin (InvivoGen, San Diego, CA).

Cell staining and imaging

MAP gels with cells cultured for 2 days were fixed in 1% paraformaldehyde for 15 minutes at 25°C. The cultures were permeabilized in 0.1% Triton X-100 in PBS and stained using DAPI (Sigma-Aldrich) for cell nuclei and rhodamine phalloidin (Thermo Fisher) for cell actin per manufacturer's guidelines for 1 hour. Gels were washed with PBS before z-stack imaging with a Nikon confocal. IMARIS was used to analyze cell spreading in z-stacks to calculate the total cell surface area from spreading after 2 days for each sample.

Transfection of MAP gel culture and assay for transgene expression

Transfection was performed two days after seeding cells in MAP gels to allow for adequate spreading. DNA polyplexes were prepared by complexing plasmid DNA encoding for Gaussia luciferase (GLuc) with jetPEI (Polyplus-Transfection, Illkirch, France) according to manufacturer's instructions. Briefly, 0.25 μg DNA was diluted in 10 μL of 150 mM NaCl and 0.5 μL jetPEI was diluted in a separate tube in 10 μL of 150 mM NaCl. The jetPEI solution was then added to the DNA solution, immediately vortexed, and allowed to incubate for 15 min at 25°C to allow for complexation. Amounts were scaled up depending on DNA dose and number of wells, but the polyplex volume administered to each well remained constant (20 μL of polyplexes were added to each well as a bolus administration). After 4 hours of polyplex exposure, the polyplex-containing media was removed and replenished with fresh media.

To verify that cells throughout the scaffold were uniformly transfected in the z-direction, plasmid DNA was mixed with the fluorescent dye, YOYO-1 (Thermo Fisher Scientific), at a ratio of 1:50 YOYO-1:base-pair DNA and was allowed to incubate for 30 min at 25°C. YOYO-1-labeled DNA was then used to prepare polyplexes as mentioned above. MAP gels containing cells and YOYO-1 polyplexes were then imaged using confocal microscopy to obtain z-stacks, and percent co-localization of YOYO-1 polyplexes with cell actin was quantified for each image based on overlapping regions of flourescence in the z-stack to

confirm consistent transfection throughout the z-direction. As described previously[25,42,43], surface area construction was performed for the polyplex and cell actin channels in the z-stacks using IMARIS, followed by using the co-localization toolbox (Manders coefficient analysis) to generate overlay regions where polyplexes and cells shared similar voxels within 0.1 um and relate to non-colocalized cell surface area. This was then displayed as a trend across each z-stack to show uniform diffusion and localization of polyplexes within the MAP void spaces.

Transfection was quantified by measuring expression of GLuc using the BioLux Gaussia Luciferase assay kit (New England Biolabs, Ipswich, MA) per manufacturer's protocol. Conditioned media was collected from each well at each time point. Briefly, 20 μL of each sample was mixed with 50 μL of substrate solution, pipetted for 2 to 3 seconds to mix, and read for luminescence with a 5 second integration time using a Modulus Fluorometer (Turner BioSystems, South San Francisco, CA). To account for transfection efficiency differences between 2-D and MAP cultures, expression data was normalized to the control group for relative transgene expression. Cell cultures were also assessed for viability using the PrestoBlue proliferation assay (Thermo Fisher Scientific) according to the manufacturer protocol. Briefly, reagent dye was diluted in 150 μL of cell media, replacing the previous media in the wells (2-D) or cell culture device (MAP). Following a 1 hour incubation at 37°C, the media was transferred to a clear 96-well plate for fluorescence measurement (excitation at 560 nm, emission at 590 nm). A blank control was subtracted as background, and the values normalized to the control for viability.

Endocytic pathway inhibition

Analysis of endocytic pathways was performed using various small molecule inhibitors (Table 1) as described in another study[15]. All inhibitors were purchased from Sigma-Aldrich.

Macropinocytosis was inhibited using 100 μM amiloride, caveolae-mediated endocytosis was inhibited using 200 μM genistein and 0.1 mM methyl-β-cyclodextrin, and clathrin-mediated endocytosis was inhibited using 10 μg/mL chlorpromazine and indirectly inhibited using 50 μM dynasore. Inhibitor pretreatment of cells was administered 2 days after seeding cells in MAP gels. For comparison to 2-D cell culture, 1.8×10^4 HDFs, which is the same number of cells seeded per 15-μL MAP gel, were seeded per well in a 48-well tissue-culture plate for 16 hours before pretreatment with inhibitors. For genistein, chlorpromazine, and amiloride, the pretreatment was administered for 0.5 and 1.5 hours for cells cultured in 2-D and MAP gels, respectively. For methyl-β-cyclodextrin and dynasore, cells were pretreated for 1 hour in both 2-D and MAP gels. After the initial pretreatment with pathway inhibitors, 0.25 μg polyplexes were added to each well for a 4-hour transfection in the presence of the inhibitors. The media was then replaced with fresh media. Transgene expression was analyzed on samples of media collected from the wells 2 days after transfection for all culture samples.

Cytoskeletal inhibition and activation

All cytoskeletal inhibitors and activators (Table 1) were purchased from Sigma-Aldrich. 20 μM cytochalasin D was used to inhibit actin polymerization, 10 μM nocodazole was used to depolymerize microtubules, and 10 mM butanedione monoxime was used to inhibit myosin ATPase. 20 nM endothelin I, 500 nM jasplakinolide, and 10μM paclitaxel were administered to activate actin/myosin, actin, and microtubule dynamics, respectively. 2-D cell cultures were prepared as described above. Pretreatment was administered for 1.5 hours for all inhibitors, 2.5 minutes for endothelin I, and 2 hours for the other activators. After the pretreatment, 0.25 μg polyplexes were added to each well for a 4-hour transfection in the presence of the inhibitors/activators. The media was then replaced with fresh media. Transgene expression was analyzed on samples of media collected from the wells 2 days after transfection.

RhoGTPase and YAP/TAZ inhibition and activation

All inhibitors and activators (Table 1) were purchased from Cytoskeleton, Inc. (Denver, CO) unless otherwise stated. RhoA, B, and C were inhibited using 1 μg/mL C3 transferase with a 4-hour pretreatment, ROCK was inhibited using 10 μM Y27632 (Selleck Chemicals, Houston, TX) for a 30-minute pretreatment, and PAK1 was inhibited using 10 μM IPA-3 (Sigma-Aldrich) for a 30-minute pretreatment. To test RhoGTPase activation, 2-D and MAP gel cultures were serum starved for 8 hours prior to 4-hour pretreatment with 1 μg/mL Rho/Rac/Cdc42 activator or 1 μg/mL Rho activator II. YAP was inhibited using 3 μM verteporfin (Sigma-Aldrich) for a 12-hour pretreatment. After the pretreatment, 0.25 μg polyplexes were added to each well for a 4-hour transfection in the presence of the inhibitors. The media was then replaced with fresh media. Transgene expression was analyzed on samples of media collected from the wells 2 days after transfection.

Statistical analysis

Statistical analysis and plotting were performed using Prism 6. Experiments were repeated two times with three to four independent gel samples in each experiment. Statistics assumed that gel samples, which were cast independently, were statistically independent from each other. All error is reported as the standard deviation of error (SD). Statistical analysis was conducted using one-way ANOVA with correction for multiple comparisons using Dunnett's post-hoc test as compared to no-treatment control for 2-D or for MAP. For each treatment, 2-D and MAP were compared to each other using unpaired two-tailed t tests.

Supplementary Material

Refer to Web version on PubMed Central for supplementary material.

Acknowledgements

We thank Nairi Tahmizyan, Mabel Chen, and Shruti Sharma for technical assistance. We also thank Talar Tokatlian for editorial assistance. We would like to acknowledge the support of funding from NIH (R01HL110592 and T32GM067555).

Abbreviations

MAP	microporous annealed particle
YAP/TAZ	Yes-associated protein / transcriptional coactivator with PDZ-binding motif
HA	hyaluronic acid
Norb	Norbornene
UV	ultraviolet
PBS	phosphate buffer saline
PEG-Tet	Polyethylene glycol – tetrazine
ROCK	Rho-associated protein kinase
MES	2-(N-morpholino)ethanesulfonic acid
RGD	Arginylglycylaspartic acid
LAP	Lithium phenyl-2,4,6-trimethylbenzoylphosphinate
TCEP	Tris(2-carboxyethyl)phosphine
DTT	Dithiothreito
PDMS	Polydimethylsiloxane
HDF	Human dermal fibroblasts
DAPI	4′,6-diamidino-2-phenylindole
GLuc	Gaussia luciferase

References

(1). Yin H; Kanasty RL; Eltoukhy AA; Vegas AJ; Robert Dorkin J; Anderson DG Non-Viral Vectors for Gene-Based Therapy. 2014 10.1038/nrg3763.

(2). Jafari M; Soltani M; Naahidi S; Karunaratne, D. N; Chen P Nonviral Approach for Targeted Nucleic Acid Delivery. Curr. Med. Chem 2012, 19 (2), 197–208. 10.2174/092986712803414141. [PubMed: 22320298]

(3). Hardee CL; Arévalo-Soliz LM; Hornstein BD; Zechiedrich L Advances in Non-Viral DNA Vectors for Gene Therapy. Genes (Basel). 2017, 8 (2), 65 10.3390/genes8020065.

(4). Kasputis T; Pannier AK The Role of Surface Chemistry-Induced Cell Characteristics on Nonviral Gene Delivery to Mouse Fibroblasts. J. Biol. Eng 2012, 6 (1), 17 10.1186/1754-1611-6-17. [PubMed: 22967455]

(5). Bengali Z; Rea JC; Shea LD Gene Expression and Internalization Following Vector Adsorption to Immobilized Proteins: Dependence on Protein Identity and Density. J. Gene Med 2007, 9 (8), 668–678. 10.1002/jgm.1058. [PubMed: 17533618]

(6). Dhaliwal A; Maldonado M; Han Z; Segura T Differential Uptake of DNA-Poly(Ethylenimine) Polyplexes in Cells Cultured on Collagen and Fibronectin Surfaces. Acta Biomater. 2010, 6 (9), 3436–3447. 10.1016/j.actbio.2010.03.038. [PubMed: 20371304]

(7). Kong HJ; Hsiong S; Mooney DJ Nanoscale Cell Adhesion Ligand Presentation Regulates Nonviral Gene Delivery and Expression. Nano Lett. 2007, 7 (1), 161–166. 10.1021/nl062485g. [PubMed: 17212457]

(8). Gojgini S; Tokatlian T; Segura T Utilizing Cell-Matrix Interactions to Modulate Gene Transfer to Stem Cells inside Hyaluronic Acid Hydrogels. Mol. Pharm 2011, 8 (5), 1582–1591. 10.1021/mp200171d. [PubMed: 21823632]

(9). Kong HJ; Liu J; Riddle K; Matsumoto T; Leach K; Mooney DJ Non-Viral Gene Delivery Regulated by Stiffness of Cell Adhesion Substrates. Nat. Mater 2005, 4 (6), 460–464. 10.1038/nmat1392. [PubMed: 15895097]

(10). Teo BKK; Goh SH; Kustandi TS; Loh WW; Low HY; Yim EKF The Effect of Micro and Nanotopography on Endocytosis in Drug and Gene Delivery Systems. Biomaterials 2011, 32 (36), 9866–9875. 10.1016/j.biomaterials.2011.08.088. [PubMed: 21924770]

(11). Tibbitt MW; Anseth KS Hydrogels as Extracellular Matrix Mimics for 3D Cell Culture. Biotechnol. Bioeng 2009, 103 (4), 655–663. 10.1002/bit.22361. [PubMed: 19472329]

(12). Griffin DR; Weaver WM; Scumpia PO; Di Carlo D; Segura T Accelerated Wound Healing by Injectable Microporous Gel Scaffolds Assembled from Annealed Building Blocks. Nat. Mater 2015, 14 (7), 737–744. 10.1038/nmat4294. [PubMed: 26030305]

(13). Sideris E; Griffin DR; Ding Y; Li S; Weaver WM; Di Carlo D; Hsiai T; Segura T Particle Hydrogels Based on Hyaluronic Acid Building Blocks. ACS Biomater. Sci. Eng 2016, 2 (11), 2034–2041. 10.1021/acsbiomaterials.6b00444.

(14). Nih LR; Sideris E; Carmichael ST; Segura T Injection of Microporous Annealing Particle (MAP) Hydrogels in the Stroke Cavity Reduces Gliosis and Inflammation and Promotes NPC Migration to the Lesion. Adv. Mater 2017, 29 (32), 1606471 10.1002/adma.201606471.

(15). Dhaliwal A; Oshita V; Segura T Transfection in the Third Dimension. Integr. Biol. (United Kingdom) 2013, 5 (10), 1206–1216. 10.1039/c3ib40086g.

(16). Dhaliwal A; Maldonado M; Lin C; Segura T Cellular Cytoskeleton Dynamics Modulates Non-Viral Gene Delivery through RhoGTPases. PLoS One 2012, 7 (4), e35046 10.1371/journal.pone.0035046. [PubMed: 22509380]

(17). Akbar H; Shang X; Perveen R; Funk K; Berryman M; Zheng Y Specific Pharmacologic Targeting of Rho GTPases Rac1, Cdc42 and RhoA Reveals Their Differential and Critical Roles In Regulation of Platelet Activation. Blood 2010, 116 (21).

(18). Nobes CD; Hall A Rho GTPases Control Polarity, Protrusion, and Adhesion during Cell Movement. J. Cell Biol 1999, 144 (6), 1235–1244. 10.1083/jcb.144.6.1235. [PubMed: 10087266]

(19). Jang J-W; Kim M-K; Bae S-C Reciprocal Regulation of YAP/TAZ by the Hippo Pathway and the Small GTPase Pathway. Small GTPases 2018, 1–9. 10.1080/21541248.2018.1435986.

(20). Ohgushi M; Minaguchi M; Sasai Y Rho-Signaling-Directed YAP/TAZ Activity Underlies the Long-Term Survival and Expansion of Human Embryonic Stem Cells. Cell Stem Cell 2015, 17 (4), 448–461. 10.1016/J.STEM.2015.07.009. [PubMed: 26321201]

(21). Dupont S; Morsut L; Aragona M; Enzo E; Giulitti S; Cordenonsi M; Zanconato F; Le Digabel J; Forcato M; Bicciato S; et al. Role of YAP/TAZ in Mechanotransduction. Nature 2011, 474 (7350), 179–184. 10.1038/nature10137. [PubMed: 21654799]

(22). Siegman S; Truong NF; Segura T Encapsulation of PEGylated Low-Molecular-Weight PEI Polyplexes in Hyaluronic Acid Hydrogels Reduces Aggregation. Acta Biomater. 2015, 28, 45–54. 10.1016/j.actbio.2015.09.020. [PubMed: 26391497]

(23). Lei Y; Rahim M; Ng Q; Segura T Hyaluronic Acid and Fibrin Hydrogels with Concentrated DNA/PEI Polyplexes for Local Gene Delivery. J. Control. Release 2011, 153 (3), 255–261. 10.1016/j.jconrel.2011.01.028. [PubMed: 21295089]

(24). Lei Y; Segura T DNA Delivery from Matrix Metalloproteinase Degradable Poly(Ethylene Glycol) Hydrogels to Mouse Cloned Mesenchymal Stem Cells. Biomaterials 2009, 30 (2), 254–265. 10.1016/j.biomaterials.2008.09.027. [PubMed: 18838159]

(25). Truong NF; Segura T Sustained Transgene Expression via Hydrogel-Mediated Gene Transfer Results from Multiple Transfection Events. ACS Biomater. Sci. Eng 2018, 4 (3), 981–987. 10.1021/acsbiomaterials.7b00957.

(26). von Gersdorff K; Sanders NN; Vandenbroucke R; De Smedt SC; Wagner E; Ogris M The Internalization Route Resulting in Successful Gene Expression Depends on Both Cell Line and Polyethylenimine Polyplex Type. Mol. Ther 2006, 14 (5), 745–753. 10.1016/j.ymthe.2006.07.006. [PubMed: 16979385]

(27). Suh J; Wirtz D; Hanes J Efficient Active Transport of Gene Nanocarriers to the Cell Nucleus. Proc. Natl. Acad. Sci 2003, 100 (7), 3878–3882. 10.1073/pnas.0636277100. [PubMed: 12644705]

(28). Grosse S; Aron Y; Thévenot G; Monsigny M; Fajac I Cytoskeletal Involvement in the Cellular Trafficking of Plasmid/PEI Derivative Complexes. J. Control. Release 2007, 122 (1), 111–117. 10.1016/j.jconrel.2007.06.015. [PubMed: 17658650]

(29). Bubb M; Spector I; Beyer B; Fosen K Effect of Jasplakinolide on the Kinetics of Actin Polymerization. J. Biol. Chem 1999, 23 (12), 2613–2621. 10.1074/jbc.275.7.5163.

(30). Ho YK; Zhou LH; Tam KC; Too HP Enhanced Non-Viral Gene Delivery by Coordinated Endosomal Release and Inhibition of β-Tubulin Deactylase. Nucleic Acids Res. 2016, 45 (6). 10.1093/nar/gkw1143.

(31). Etienne-Manneville S; Hall A Rho GTPases in Cell Biology. Nature 2002, 420 (6916), 629–635. 10.1038/nature01148. [PubMed: 12478284]

(32). Akbar H; Duan X; Saleem S; Davis AK; Zheng Y RhoA and Rac1 GTPases Differentially Regulate Agonist-Receptor Mediated Reactive Oxygen Species Generation in Platelets. PLoS One 2016, 11 (9), e0163227 10.1371/journal.pone.0163227. [PubMed: 27681226]

(33). Szczepanowska J Involvement of Rac/Cdc42/PAK Pathway in Cytoskeletal Rearrangements. Acta Biochim. Pol 2009, 56 (2), 225–234. [PubMed: 19513348]

(34). Tang DD; Gunst SJ The Small GTPase Cdc42 Regulates Actin Polymerization and Tension Development during Contractile Stimulation of Smooth Muscle. J. Biol. Chem 2004, 279 (50), 51722–51728. 10.1074/jbc.M408351200. [PubMed: 15456777]

(35). Szeto SG; Narimatsu M; Lu M; He X; Sidiqi AM; Tolosa MF; Chan L; De Freitas K; Bialik JF; Majumder S; et al. YAP/TAZ Are Mechanoregulators of TGF-β-Smad Signaling and Renal Fibrogenesis. J. Am. Soc. Nephrol 2016, 27 (10), 3117–3128. 10.1681/ASN.2015050499. [PubMed: 26961347]

(36). Caliari SR; Vega SL; Kwon M; Soulas EM; Burdick JA Dimensionality and Spreading Influence MSC YAP/TAZ Signaling in Hydrogel Environments. Biomaterials 2016, 103, 314–323. 10.1016/J.BIOMATERIALS.2016.06.061. [PubMed: 27429252]

(37). Liu F; Lagares D; Choi KM; Stopfer L; Marinković A; Vrbanac V; Probst CK; Hiemer SE; Sisson TH; Horowitz JC; et al. Mechanosignaling through YAP and TAZ Drives Fibroblast Activation and Fibrosis. Am. J. Physiol. - Lung Cell. Mol. Physiol 2015, 308 (4), L344–L357. 10.1152/ajplung.00300.2014. [PubMed: 25502501]

(38). Wang C; Zhu X; Feng W; Yu Y; Jeong K; Guo W; Lu Y; Mills GB Verteporfin Inhibits YAP Function through Up-Regulating 14-3-3σ Sequestering YAP in the Cytoplasm. Am J Cancer Res 2016, 6 (1), 27–37. [PubMed: 27073720]

(39). Kim J; Jo H; Hong H; Kim MH; Kim JM; Lee J-K; Heo W. Do; Kim J Actin Remodelling Factors Control Ciliogenesis by Regulating YAP/TAZ Activity and Vesicle Trafficking. Nat. Commun 2015, 6 (1), 6781 10.1038/ncomms7781. [PubMed: 25849865]

(40). Zanconato F; Forcato M; Battilana G; Azzolin L; Quaranta E; Bodega B; Rosato A; Bicciato S; Cordenonsi M; Piccolo S Genome-Wide Association between YAP/TAZ/TEAD and AP-1 at Enhancers Drives Oncogenic Growth. Nat. Cell Biol 2015, 17 (9), 1218–1227. 10.1038/ncb3216. [PubMed: 26258633]

(41). Piccolo S; Dupont S; Cordenonsi M The Biology of YAP/TAZ: Hippo Signaling and Beyond. Physiol. Rev 2014, 94 (4), 1287–1312. 10.1152/physrev.00005.2014. [PubMed: 25287865]

(42). Hwang ME; Keswani RK; Pack DW Dependence of PEI and PAMAM Gene Delivery on Clathrin- and Caveolin-Dependent Trafficking Pathways. Pharm. Res 2015, 32 (6), 2051–2059. 10.1007/s11095-014-1598-6. [PubMed: 25511918]

(43). Gaspar VM; Baril P; Costa EC; de Melo-Diogo D; Foucher F; Queiroz JA; Sousa F; Pichon C; Correia IJ Bioreducible Poly(2-Ethyl-2-Oxazoline)–PLA–PEI-SS Triblock Copolymer Micelles

for Co-Delivery of DNA Minicircles and Doxorubicin. J. Control. Release 2015, 213, 175–191. 10.1016/J.JCONREL.2015.07.011. [PubMed: 26184050]

(44). Liu-Chittenden Y; Huang B; Shim JS; Chen Q; Lee S-J; Anders RA; Liu JO; Pan D Genetic and Pharmacological Disruption of the TEAD-YAP Complex Suppresses the Oncogenic Activity of YAP. Genes Dev. 2012, 26 (12), 1300–1305. 10.1101/gad.192856.112. [PubMed: 22677547]

(45). Zhang H; Ramakrishnan SK; Triner D; Centofanti B; Maitra D; Győrffy B; Sebolt-Leopold JS; Dame MK; Varani J; Brenner DE; et al. Tumor-Selective Proteotoxicity of Verteporfin Inhibits Colon Cancer Progression Independently of YAP1. Sci. Signal 2015, 8 (397), ra98 10.1126/scisignal.aac5418. [PubMed: 26443705]

(46). Lin C-H; Pelissier FA; Zhang H; Lakins J; Weaver VM; Park C; LaBarge MA Microenvironment Rigidity Modulates Responses to the HER2 Receptor Tyrosine Kinase Inhibitor Lapatinib via YAP and TAZ Transcription Factors. Mol. Biol. Cell 2015, 26 (22), 3946–3953. 10.1091/mbc.E15-07-0456. [PubMed: 26337386]

(47). Zanconato F; Battilana G; Cordenonsi M; Piccolo S YAP/TAZ as Therapeutic Targets in Cancer. Curr. Opin. Pharmacol 2016, 29, 26–33. 10.1016/J.COPH.2016.05.002. [PubMed: 27262779]

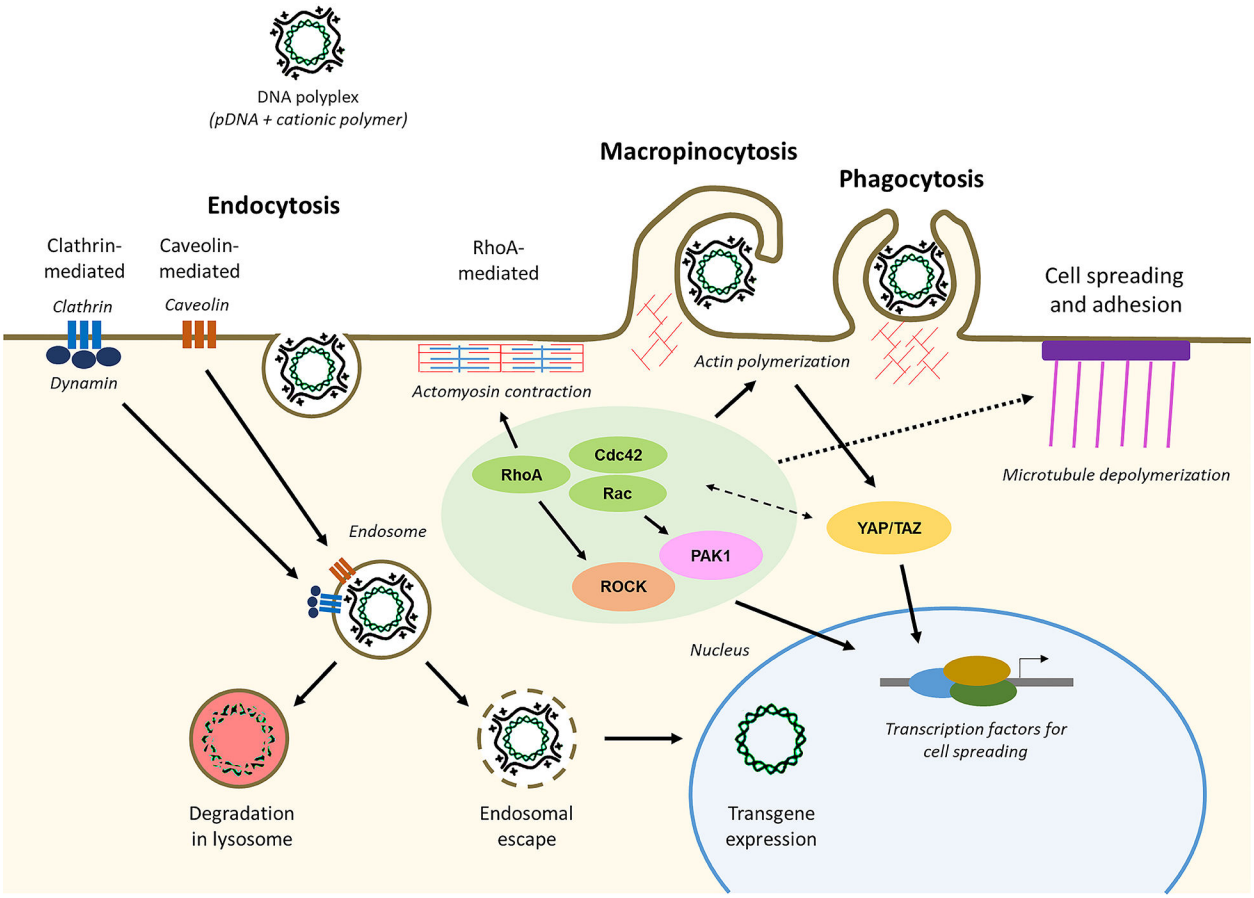

Figure 1.

Polyplex internalization pathways, driven by mediators, cytoskeleton movements, and GTPase signaling. While many more pathways influence those shown, in addition to feedback control from extracellular and intracellular factors, the simple overview highlights the key mechanisms of interest and methods for inhibition or activation for know effectors RhoA, Rac, and Cdc42[16–18]. The YAP/TAZ pathway was also explored as past studies have shown a possible relation between Rho and actin polymerization regulation through YAP[19–21]. Note that bold arrows indicate the general flow for cascades as it related to polyplex uptake and processing or membrane resturcturing, with dotted arrows indicating cross-pathway interactions between different cascades.

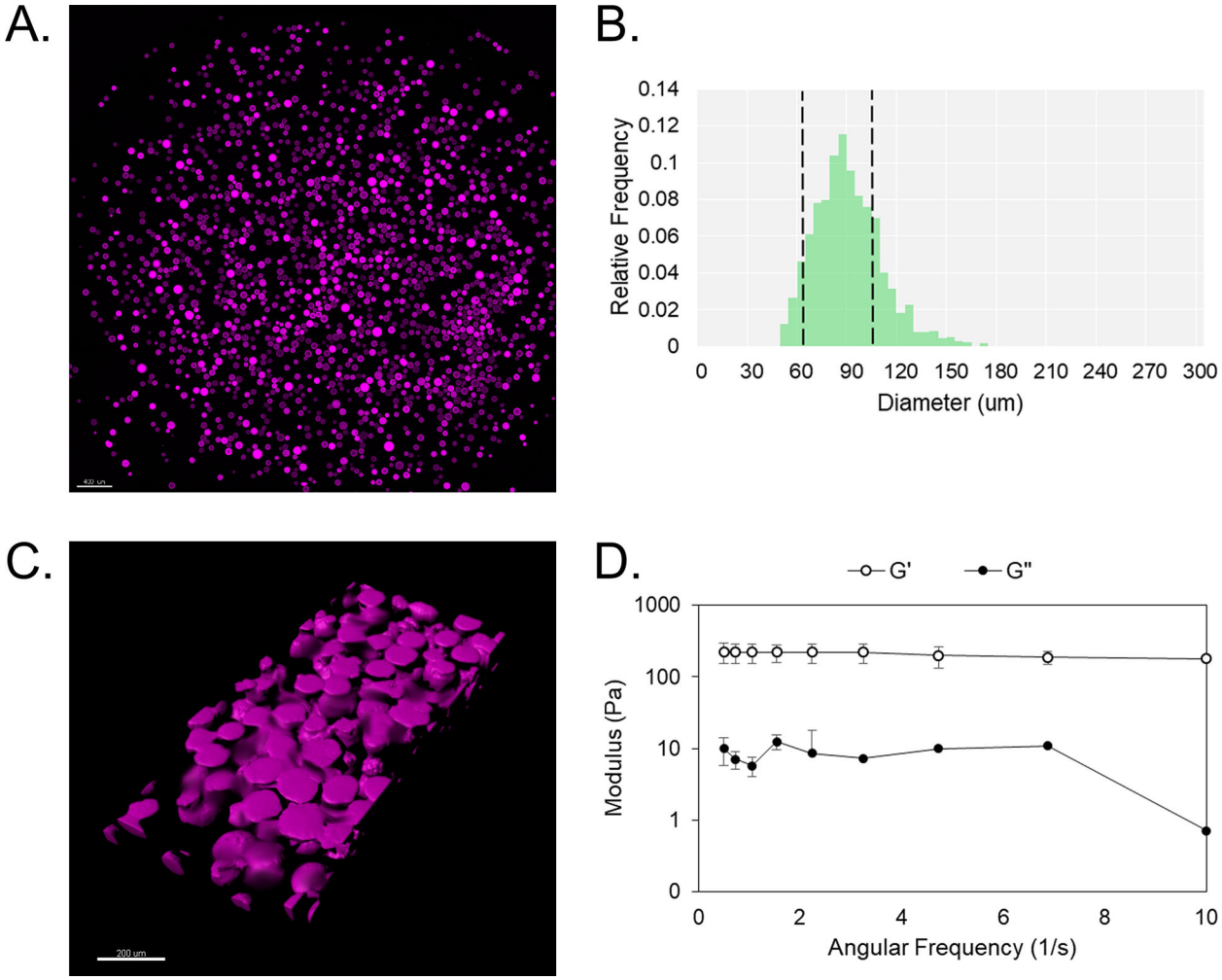

Figure 2.

Characterization of MAP gel formation and scaffold properties. (A) Imaging of stained MAP gel from bulk mixing, used to determine size in ImageJ from binary. Scale bar = 400 um. (B) Size distribution of MAP gel diameters for 60–100 um sieve, binned at intervals of 5 from 0–300 um. Dashed lines indicate filter pore size. (C) 3-D image of annealed MAP scaffold. IMARIS was used to generate a volume render of the gel. Scale bar = 200 μm. (D) Rheological properties of the scaffold, with storage modulus, G', and loss modulus, G", for a given angular frequency.

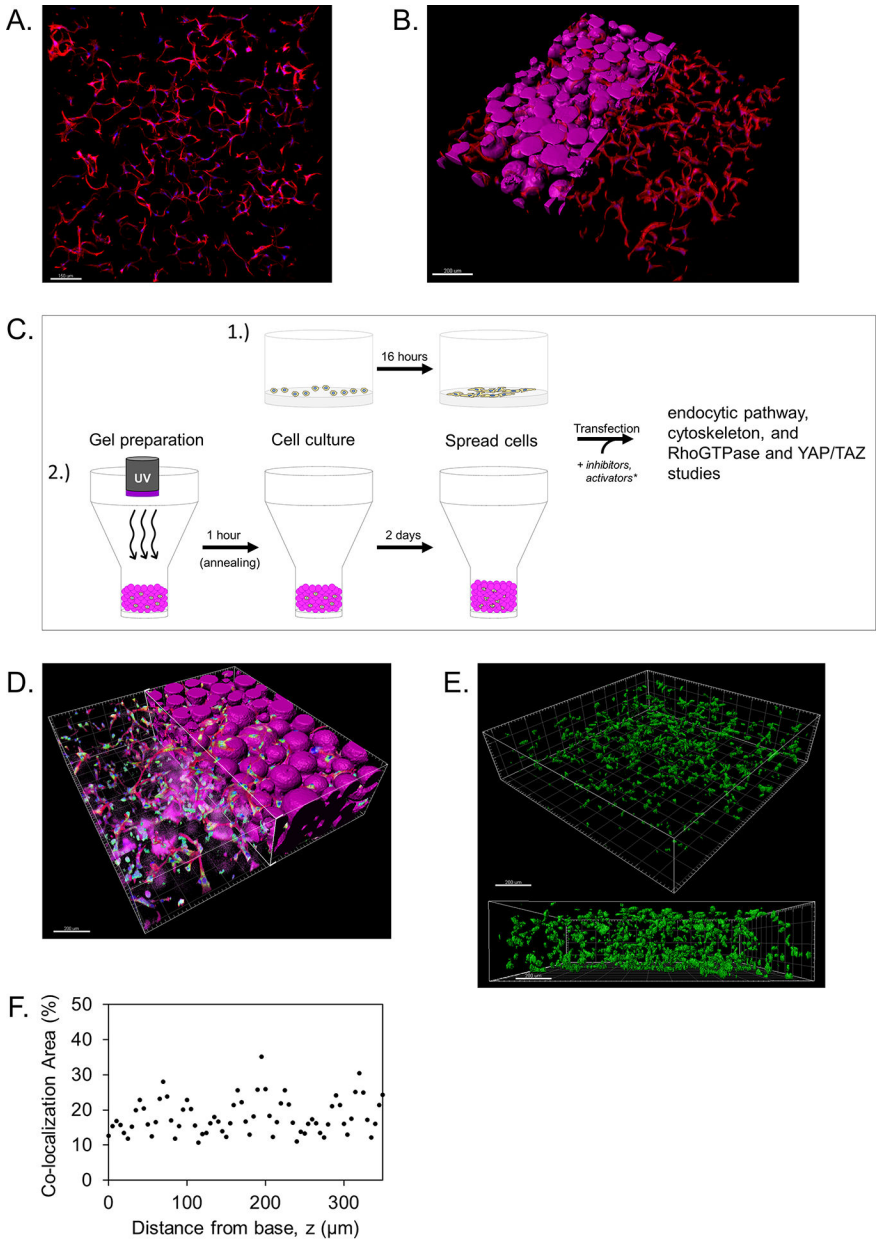

Figure 3.

Characterization of HDF cell culture and transfection in MAP gels. (A) 2-D confocal image of single z-stack for HDF cells (actin in red, nuclei in blue) cultured in MAP gels 2 days after initial seeding. Scale bar = 150 μm. (B) 3-D rendering of z-stacks of HDFs cultured in MAP gels 2 days after seeding. IMARIS was used to generate a volume render of the MAP gel of the left half of the image. Scale bar = 200 μm. (C) Overview of cell culture and transfection methods, with 1.) traditional 2-D (plate) transfection, and 2.) 3-D MAP transfection. *Note that the order and incubation time for inhibitor and polyplex addition varied per study (refer to Methods and Table 1). (D) 3-D rendering of cells 4 hours after transfection, with a cutaway showing the presence of YOYO-1 stained polyplexes and phalloidin/DAPI stained cells. Scale bar = 200 μm. (E) Gel rendering with only the space

occupied by polyplexes visualized in a 3-D and side view, showing homogeneous distribution throughout the scaffold. Scale bar = 200 μm. (F) Quantification of polyplex distribution relative to phalloidin-stained actin for cells through the total z-stack, based on the cell surface area and overlapping regions with polyplexes.

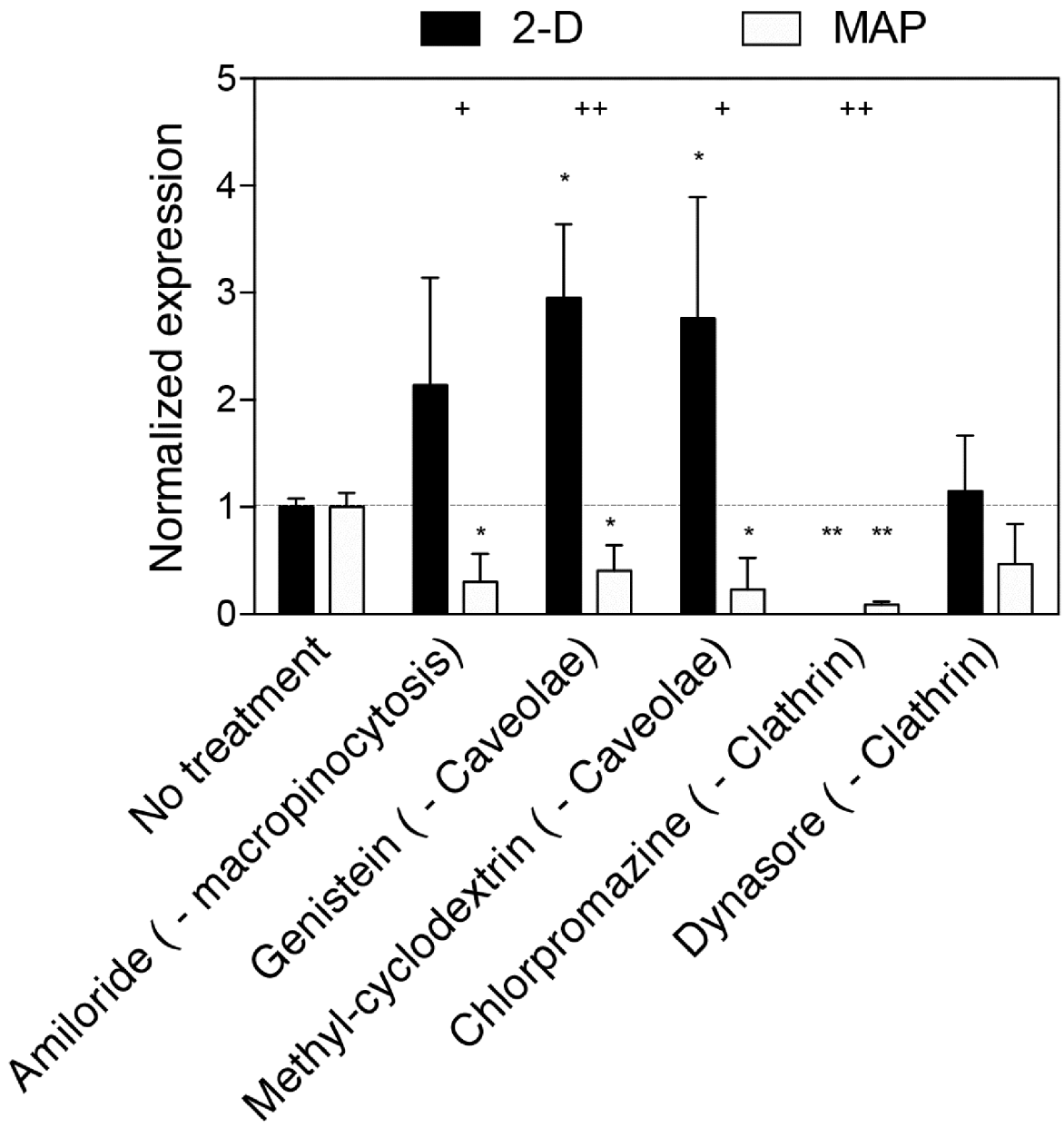

Figure 4.

Effects of endocytic inhibitors on transgene expression 2 days after bolus transfection with polyplexes of HDFs cultured on tissue culture plastic (2-D) or in MAP gels. Statistical analysis was conducted using one-way ANOVA with correction for multiple comparisons using Dunnett's post-hoc test (* $p < 0.05$, ** $p < 0.01$, and *** $p < 0.001$) as compared to no-treatment control for 2-D or for MAP. For each treatment, 2-D and MAP were compared to each other using unpaired two-tailed t tests ($^{+}$ $p < 0.05$, $^{++}$ $p < 0.01$, and $^{+++}$ $p < 0.001$).

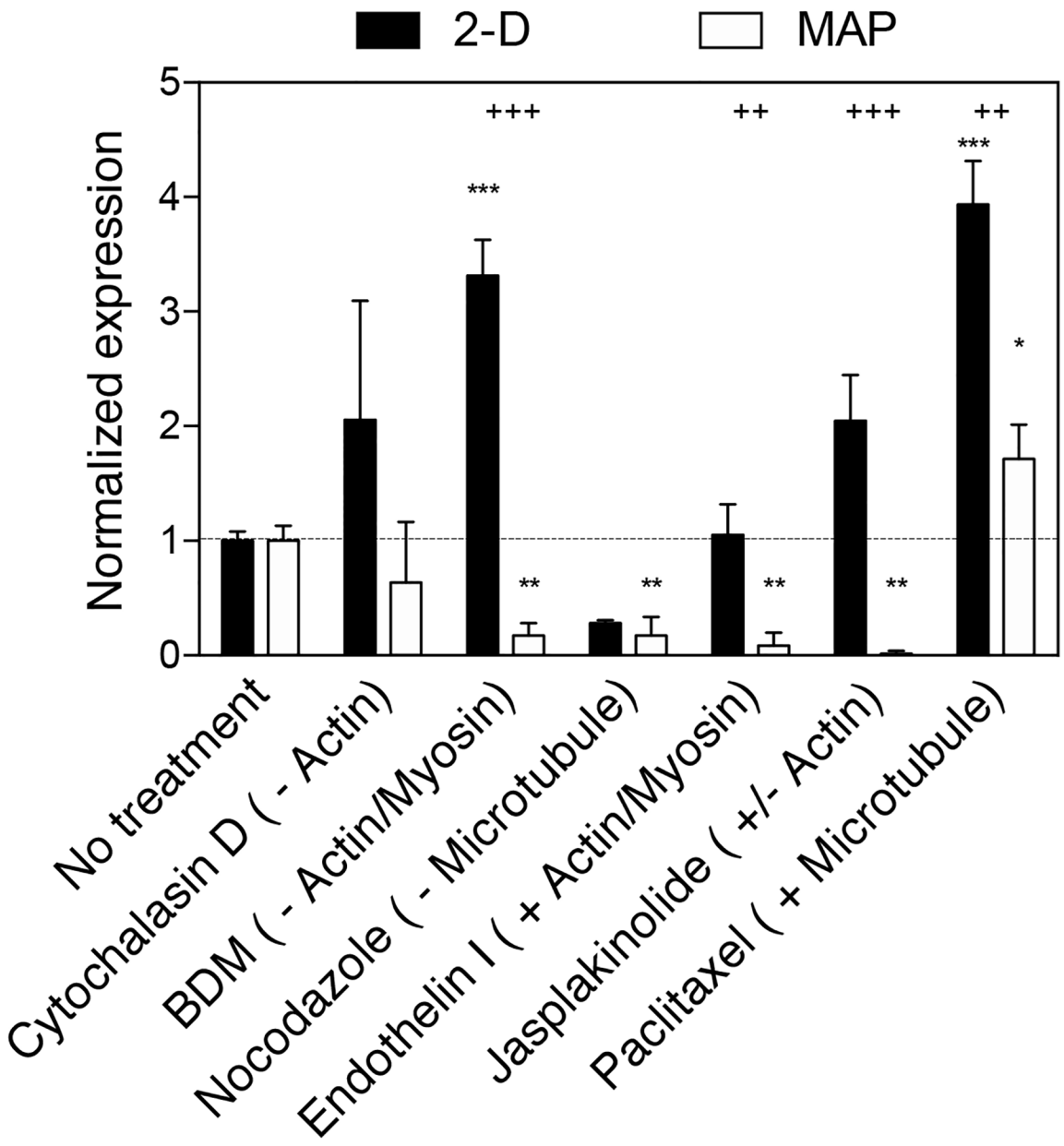

Figure 5.

Effects of cytoskeletal inhibitors and activators on transgene expression 2 days after transfection. Statistical analysis was conducted using one-way ANOVA with correction for multiple comparisons using Dunnett's post-hoc test (* $p < 0.05$, ** $p < 0.01$, and *** $p < 0.001$) as compared to no-treatment control for 2-D or for MAP. For each treatment, 2-D and MAP were compared to each other using unpaired two-tailed t tests ($^{+}$ $p < 0.05$, $^{++}$ $p < 0.01$, and $^{+++}$ $p < 0.001$).

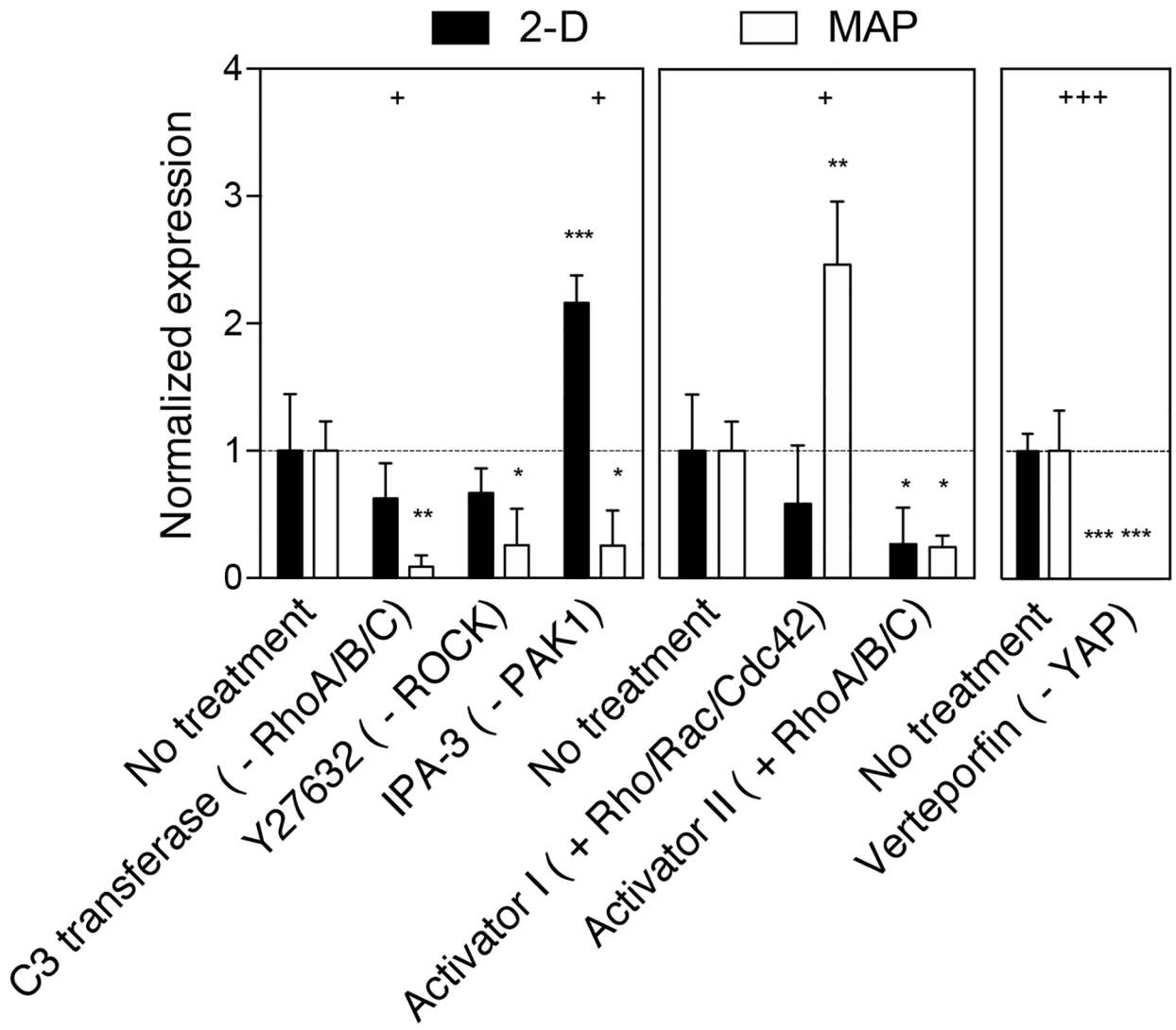

Figure 6.

Effects of inhibitors and activators of RhoGTPases and inhibition of YAP on transgene expression 2 days after transfection. Statistical analysis was conducted using one-way ANOVA with correction for multiple comparisons using Dunnett's post-hoc test (* $p < 0.05$, ** $p < 0.01$, and *** $p < 0.001$) as compared to no-treatment control for 2-D or for MAP. For each treatment, 2-D and MAP were compared to each other using unpaired two-tailed t tests ($^{+}$ $p < 0.05$, $^{++}$ $p < 0.01$, and $^{+++}$ $p < 0.001$).

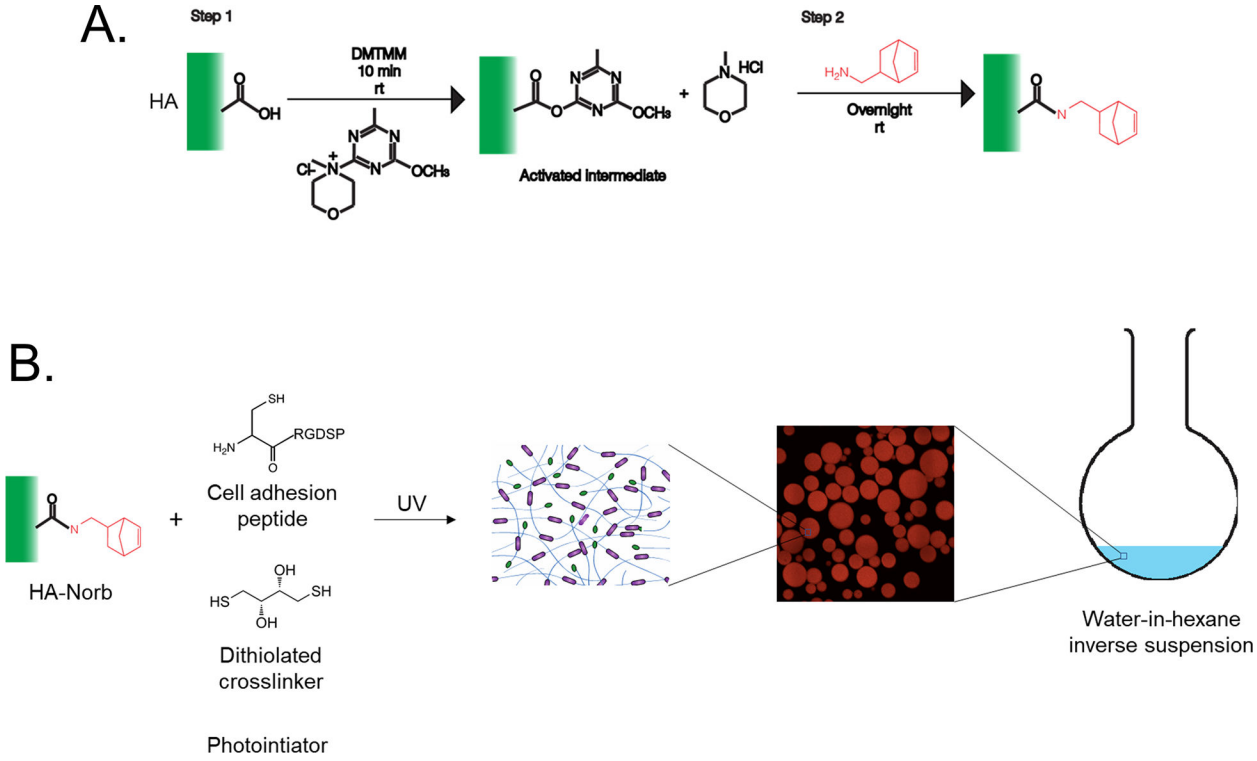

Figure 7.

Microgel production for MAP. (A) Formation of hyaluronic acid – nobornene (HA-Norb). (B) Addition of RGD peptide and DTT crosslinking of HA-Norb to form MAP gels.

Table 1.

Overview of inhibitors and activators for internalization, contractility, and signalling pathways. Note that the time of treatment refers to the duration for drug exposure before 0.25 uM polyplexes were added to the solution. Media was replaced only after the 4-hour polyplex incubation time. *Specific for the RhoGTPase activators, pretreatment was in serum-free media.

Drug	Target	Function	Concentration	Time of treatment	
				2-D culture	*MAP culture*
Chlorpromazine	Clathrin	Inhibitor	10 ug/mL	0.5 hours	1.5 hours
Dynasore	Dynamin (indiretly clathrin)	Inhibitor	50 uM	1 hour	
Genistein	Caveolae	Inhibitor	200 uM	0.5 hours	1.5 hours
Methyl-β-cyclodextrin	Caveolae	Inhibitor	0.1 mM	1 hour	
Amiloridae	Macropinocytosis	Inhibitor	100 uM	0.5 hours	1.5 hours
Cytochalasin D	Actin polymerization	Inhibitor	20 uM	1.5 hours	
Nocodazole	Microtubule depolymerization	Inhibitor	10 uM	1.5 hours	
Butanedione monoxime	Myosin-ATPase	Inhibitor	10 mM	1.5 hours	
Jasplakinolide	Actin polymerization	Activator	500 nM	2 hours	
Paclitaxel	Microtubule depolymerization	Activator	10 uM	2 hours	
Endothelin I	Myosin-ATPase	Activator	20 uM	2.5 min	
C3 transferase	Rho	Inhibitor	1 ug/mL	4 hour	
Verteporfin	YAP/TAZ	Inhibitor	3 uM	12 hours	
IPA-3	PAK1 (indirectly Rac, Cdc42)	Inhibitor	10 uM	30 min	
Y27632	ROCK (indirectly RhoA)	Inhibitor	10 uM	30 min	
Rho/Rac/Cdc42 activator	Rho, Rac, Cdc42	Activator	1 ug/mL	12 hours*	
Rho director activator II	Rho	Activator	1 ug/mL	12 hours*	